SSRG International Journal of Civil Engineering
ISSN: 2348-8352/ https://doi.org/10.14445/23488352/IJCE-V13I10P115

Volume 13 Issue 10, 241-256, October 2026
© 2026 Seventh Sense Research Group®

Original Article

Performance Assessment of Fe-Fe Punched and Mesh Electrodes in EC and AEC Treatment of Distillery Spent Wash

Pooja P[1], Lokeshappa B[2], Rashma Shetty[3], Anil Kumar B.S[4]

[1,2,3,4]*Department of Studies in Civil Engineering, University B.D.T College of Engineering, Davanagere, Karnataka, India,*
[1,2,3,4]*Visvesvaraya Technology University, Belagavi, India.*

[1]*Corresponding Author: poojapnaik018@gmail.com*

Received: 27 May 2026 Revised: 27 August 2026 Accepted: 02 September 2026 Published: 28 October 2026

Abstract *- Distillery Spent Wash (DSW) is a highly contaminated wastewater that is difficult to treat because it contains dissolved salts, organic materials, and melanoidins. This study assesses the effectiveness of Electrocoagulation (EC) and Aerated Electrocoagulation (AEC) using Iron-Iron (Fe-Fe) punched and mesh electrodes for the treatment of DSW. Response Surface Methodology (RSM) based on a Box-Behnken Design (BBD) was used to improve operational parameters such as Electrolysis Time (ET) (30–120 min), Voltage (V) (10-30 V), Electrode Distance (ED) (1.5-2.5 cm), and Agitation Speed (AS) (300–900 rpm). The findings showed 70–91% color removal, 60–91% Chemical Oxygen Demand (COD) reduction, and 50–89% Total Dissolved Solids (TDS) removal. Because of improved oxidation and flocculation processes, AEC showed greater treatment efficiency than EC. Among the electrode configurations, Fe–Fe mesh electrodes under AEC conditions showed the highest removal performance. Scanning Electron Microscopy (SEM) analysis revealed surface roughening and oxide–hydroxide layer formation on the electrodes after treatment, while Energy-Dispersive X-ray Spectroscopy (EDX) confirmed increased oxygen content and adsorption of spentwash-derived ions. Economic analysis indicated that both EC and AEC are cost-effective, with operating costs of ₹54.46/m³ and ₹54.48/m³, respectively. Overall, the study confirms that EC and AEC using Fe–Fe electrodes are efficient and economical treatment methods for DSW.*

Keywords *- Aerated Electrocoagulation, Distillery Spent Wash, Electrocoagulation, Iron electrode, Punched electrode.*

1. Introduction

Distillery Spent Wash (DSW), one of the most heavily contaminated industrial wastewaters because of its high concentrations of organic matter, melanoidins, dissolved salts, and acidic character, has been produced at a much higher rate as a result of the distillery industry's fast rise (Damaraju et al. 2019; Khokhar et al. 2023; Krishna et al. 2010). The presence of recalcitrant melanoidins imparts an intense dark brown colour to DSW, reducing light penetration in receiving water bodies and causing severe environmental problems, including oxygen depletion and deterioration of aquatic ecosystems (Bezuneh et al. 2016; Singh et al. 2020). Thus, DSW treatment remains an environmental issue demanding effective and sustainable technology.

Traditional distillery wastewater treatment comprises anaerobic digestion and aerobic biological treatment to decrease biodegradable organic debris (Rahul et al. 2021; Thakur et al. 2009). Although biological processes effectively decrease biochemical oxygen demand, they are often insufficient for removing residual colour, refractory organic compounds, and dissolved solids remaining in biomethanated spentwash (Kumar et al., 2009). Therefore, advanced electrochemical treatment methods have gained considerable attention as polishing processes to achieve stringent discharge standards. Among the available electrochemical technologies, EC has emerged as an efficient and environmentally friendly treatment process because it generates coagulant species in situ without the addition of external chemicals. During EC, sacrificial iron electrodes dissolve under an applied electric current, producing ferrous and ferric hydroxide species that effectively destabilize colloidal particles and adsorb dissolved organic pollutants through charge neutralization, sweep coagulation, and flotation mechanisms (Jing et al., 2023). AEC further enhances the EC process by supplying oxygen, which accelerates the oxidation of Fe^{2+} to Fe^{3+}, improves mass transfer, minimizes electrode passivation, and promotes the formation and flotation of pollutant flocs (Emamjomeh and Sivakumar, 2009; Nidheesh et al. 2020; Nidheesh and Omur, 2023). Ozone, Fenton and photo-Fenton processes, photocatalysis, and UV-assisted oxidation have also been studied for DSW treatment because they generate highly

This is an open access article under the CC BY-NC-ND license (http://creativecommons.org/licenses/by-nc-nd/4.0/)

reactive oxidizing species and degrade recalcitrant organic compounds and color-causing constituents (Verma et al., 2021). Hybrid electrochemical systems have been studied to enhance industrial wastewater treatment. Using aerated EC and modified peroxi-coagulation, Abhijeet et al. (2018) showed that EC may be combined with other oxidation processes to improve pollutant removal.

Several researchers have successfully applied EC and AEC for the treatment of DSW using different electrode materials and reactor configurations. The positive impact of electrode alteration on treatment performance was shown by Shanmukha et al. (2020), who examined bare and punched aluminum and iron electrodes under aerated conditions and observed color and COD removal efficiencies of around 80–88% and 75–85%, respectively. Charles and Arunnellaiappan (2022) employed twisted iron electrodes and achieved a maximum colour removal efficiency of 83.75% under optimized operating conditions. Khokhar et al. (2023) adjusted electrochemical treatment settings and achieved color and COD removal efficiencies higher than 90% under optimum process conditions, whereas an Al–SS–Al electrode configuration was investigated for anaerobically digested DSW and reported COD removal surpassing 80%. These investigations demonstrate the effectiveness of electrochemical treatment technologies for treating high-strength distillery wastewater. Khandegar and Saroha (2012) investigated different combinations of aluminium and iron electrodes for the electrochemical treatment of DSW and reported a maximum COD removal of 81.3% using Al–Al electrodes under optimized operating conditions, demonstrating the influence of electrode material on treatment performance. David et al. (2025) investigated aluminum-electrode-based EC combined with nano-Al_2O_3 adsorption and reported colour and COD removals of 94.42% and 99.1%, respectively, demonstrating the potential of integrating EC with adsorption for enhanced treatment of distillery effluent.

Despite the increasing application of EC for distillery spentwash treatment, limited information is available regarding the comparative performance of Fe–Fe punched and Fe–Fe mesh electrode configurations under both EC and AEC operating conditions. Furthermore, it is unusual for prior research to combine electrode surface characterization, techno-economic assessment, and process optimization utilizing RSM in a single experimental framework. Despite previous studies, the role of electrode shape in influencing operating cost, electrode surface changes, and pollutant removal efficiency remains insufficiently understood. By comparing Fe–Fe punched and Fe–Fe mesh electrode designs for the treatment of distillery spentwash utilizing both EC and aerated EC, the current study fills in these information gaps. Response Surface Methodology, which is based on a Box-Behnken Design, was used to optimize the impacts of electrolysis duration, applied voltage, inter-electrode spacing, and agitation speed. The study investigates electrode surface changes using SEM and EDX analyzes, evaluates color, COD, and Total Dissolved Solids (TDS) removal efficiency, and evaluates the operational costs of EC and AEC processes. This integrated method offers a thorough knowledge of how electrode geometry affects process economics, treatment efficiency, and the usefulness of electrochemical treatment for high-strength industrial wastewater.

2. Materials and Methodology

2.1. Materials

The DSW came from Samson's Distilleries in Duggavathi, Davanagere, Karnataka, India. To reduce physicochemical changes, the wastewater samples were brought to the lab in 20-liter polypropylene containers and kept at 4°C until further examination. The effluent was diluted with deionized water to achieve the necessary working concentration prior to testing.

Physicochemical parameters of wastewater were assessed using the Standard Methods for the Examination of Water and Wastewater (APHA, 2012), including pH, color, COD, BOD^2, TDS, and chloride content. Color was determined at 475 nm using a UV–visible spectrophotometer (Model DR2007, HACH, USA). Changes in the elemental composition of the electrodes were evaluated by Energy-Dispersive X-ray Spectroscopy (EDX), while scanning electron microscopy (SEM; Hitachi SU3500) was used to examine the electrode surface morphology before and after treatment. Before SEM imaging, an Edwards S150 sputter coater gold-coated the electrode surfaces to boost electrical conductivity. Pal Scientific Pvt. Ltd. in Davanagere, India, supplied all analytical-grade chemicals for the study.

2.2. Experimental Setup

EC and AEC experiments were done in a 2 L batch glass reactor with a 1.5 L effective working capacity. To assess the impact of electrode geometry on treatment performance, two Fe–Fe electrode configurations, punched and mesh electrodes, were examined. Each electrode was placed vertically in a parallel configuration and had dimensions of 15 cm by 5 cm. The mesh electrode's effective surface area was 18.50 cm^2, whereas the punched electrode's was 48.42 cm^2. Throughout the experiments, the plain electrode served as the cathode, whereas the punched or mesh electrode functioned as the sacrificial anode. The punched electrode was selected because the perforations enhance local turbulence, improve electrolyte circulation, and facilitate uniform current distribution, thereby promoting efficient coagulant generation. In contrast, the mesh electrode provides a highly interconnected structure that enhances mass transfer, increases the availability of electrochemically active sites, and reduces concentration polarisation near the electrode surface. Comparing these two geometries enables evaluation of how electrode surface influences pollutant removal efficiency under identical operating conditions. A diffuser was used to constantly provide compressed air at a constant aeration rate of 1.5 L

min^{-1} for AEC studies. Aeration improves dissolved oxygen availability, accelerates the oxidation of Fe^{2+} to Fe^{3+}, suppresses electrode passivation, and enhances the flotation of pollutant-laden flocs, thereby improving overall treatment efficiency. The experimental setup used for both electrode configurations is illustrated in Figure 1.

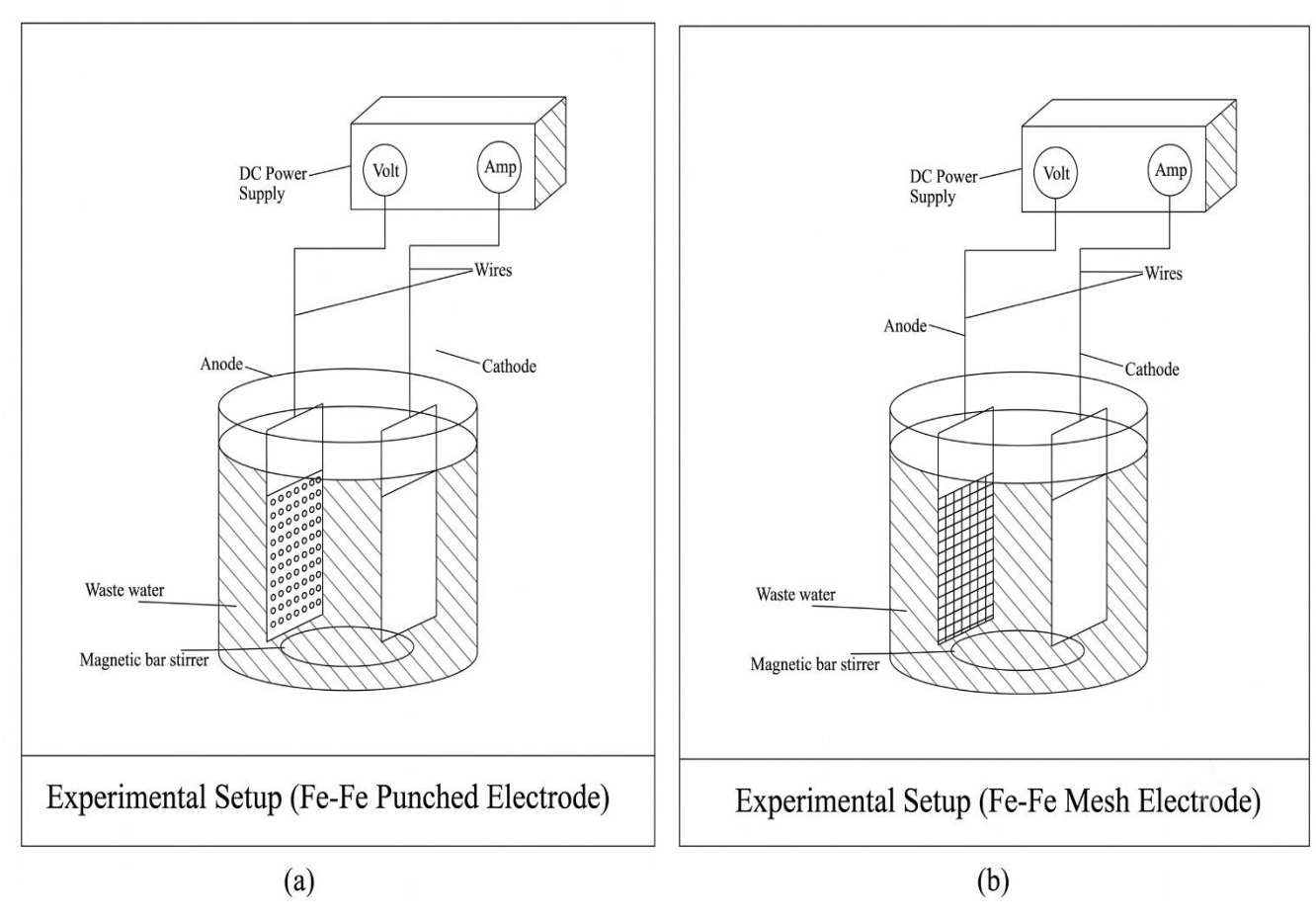


Fig. 1 Experimental setup, (a) Punched electrode, and (b) Mesh electrode.

For this study, a 1.5 L laboratory batch reactor was employed. Therefore, the results demonstrate the treatment performance of the Fe–Fe punched and mesh electrode configurations under controlled laboratory conditions, but do not directly establish their performance at larger scales. Scale-up of the process would require further evaluation of parameters such as reactor volume, electrode area-to-volume ratio, current density, electrode spacing, mixing, aeration requirements, energy consumption, and sludge generation. Therefore, continuous-flow pilot-scale experiments are needed to confirm that the improved operating conditions at greater treatment capacity are both economically feasible and practically applicable.

2.3. Experimental Design and Statistical Analysis

The EC and AEC processes were optimized, and the interaction effects of operational factors on pollutant removal were assessed, using RSM based on a BBD. Based on initial research and prior studies showing their substantial impact on electrochemical treatment performance, four independent variables were chosen: electrolysis time (30–120 min), inter-electrode distance (1.5–2.5 cm), applied voltage (10–30 V), and agitation speed (300–900 rpm). Table 1 lists the independent variables along with the associated levels.

A four-factor, three-level BBD generated 27 experimental runs using Minitab 19 software, as shown in Table 2. The responses investigated were the percentage removal of colour, Chemical Oxygen Demand (COD), and Total Dissolved Solids (TDS). Regression equations were developed to establish the relationships between the operating variables and treatment efficiencies. ANOVA was used to assess the regression models' statistical significance and appropriateness. The F-value and p-value were used to evaluate model significance, while R^2 and Adjusted R^2 were used to evaluate regression model goodness-of-fit. To validate the models, experimental findings were compared to model predictions.

Table 1. Considerations for the experimental design (Independent variable)

Factor	Symbol	Unit	Low level (-1)	High level (+1)
Electrolysis time	A	min	30	120
Inter-electrode distance	B	cm	1.5	2.5
Applied voltage	C	V	10	30
Agitation Speed	D	rpm	300	900

Table 2. Trial run of RSM from Minitab 19

Std Order	Run Order	ET	ED	Voltage	RPM
6	1	75	2	30	300
16	2	75	2.5	30	600
7	3	75	2	10	900
19	4	30	2	30	600
1	5	30	1.5	20	600
22	6	75	2.5	20	300
12	7	120	2	20	900
21	8	75	1.5	20	300
25	9	75	2	20	600
9	10	30	2	20	300
5	11	75	2	10	300
24	12	75	2.5	20	900
20	13	120	2	30	600
18	14	120	2	10	600
3	15	30	2.5	20	600
27	16	75	2	20	600
14	17	75	2.5	10	600
13	18	75	1.5	10	600
17	19	30	2	10	600
2	20	120	1.5	20	600
8	21	75	2	30	900
15	22	75	1.5	30	600
4	23	120	2.5	20	600
23	24	75	1.5	20	900
26	25	75	2	20	600
11	26	30	2	20	900
10	27	120	2	20	300

3. Results and Discussion

3.1. Optimization of Colour Removal Efficiency

Table 3 shows the DSW's fundamental physicochemical parameters from this study. A four-factor, three-level BBD-based RSM improved color removal trials.

Appendix 1 (Tables 5 and 6) contains the ANOVA results, while Table 4 shows the Fe–Fe pierced and mesh electrode color removal efficiencies. The color removal percentage was calculated using Equation (1).

$$\text{Percentage removal} = \frac{100(initial\ value - Final\ value)}{Initial\ value} \quad (1)$$

Table 3. Initial characteristics of Distillery Spent Wash

Parameter	Initial Value	Unit	Methods
pH	4.0	—	Electrometric
(TDS)	38,550	mg/L	Electrometric
Chlorides	5,400	mg/L	Volumetric
Colour	48,075	Pt-Co	Spectrophotometric
(COD)	84,800	mg/L	Open Reflex
(BOD_5)	42,075	mg/L	Winkler titrimetric

The link between the operational variables and color removal efficiency was sufficiently explained by the fitted quadratic models. Additionally, Analysis of Variance (ANOVA) revealed that although inter-Electrode Distance (ED) and Agitation Speed (AS) showed relatively minor or model-dependent impacts, Electrolysis Time (ET) and applied Voltage (V) substantially impacted color removal ($p < 0.05$).

For the Fe–Fe punched electrode, the regression models exhibited F-values of 161.38 for EC and 39.17 for AEC, whereas the corresponding models for the Fe–Fe mesh electrode showed F-values of 241.23 and 134.90, respectively. In all cases, the models were statistically significant ($p < 0.0001$), confirming that the developed regression equations satisfactorily represented the experimental observations. The created response surface models' adequacy and predictive power are further supported by the good agreement between the actual and model-predicted color removal efficiency (Table 4). Equations (2) through (5) provide the final regression equations that describe color removal for the Fe–Fe punched and mesh electrodes. Final Regression equations for Fe-Fe (Punched-Plain and Mesh-Plain)

$$Colour_{EC\ (punched)} = 74.31 + 0.1768\ ET - 3.93\ ED + 0.112\ V - 0.02516\ RPM + 0.000073\ ET*ET + 0.23\ ED*ED + 0.00611\ V*V + 0.000014\ RPM*RPM - 0.0001\ ET*ED - 0.001711ET*V + 0.000007ET*RPM - 0.0220\ ED*Voltage + 0.00545ED*RPM + 0.000042*RPM \quad (2)$$

$$Colour_{AEC(punched)} = 52.78 + 0.1737\ ET + 9.34\ ED + 0.487\ V + 0.00276\ RPM - 0.000155\ ET*ET - 1.08\ ED*ED - 0.00125\ V*V - 0.000003\ RPM*RPM - 0.0607\ ET*ED + 0.000189\ ET*V + 0.000016\ ET*RPM - 0.0820\ ED*V + 0.00057\ ED*RPM - 0.000045\ V*RPM \quad (3)$$

$$Colour_{EC(mesh)} = 91.37 + 0.1449\ ET - 17.02\ ED + 0.409\ V + 0.01889\ RPM + 0.000005\ ET*ET + 2.31\ ED*ED + 0.00026\ V*V - 0.000007\ RPM*RPM - 0.0524\ ET*ED - 0.000167\ ET*V - 0.000019\ ET*RPM - 0.1415\ ED*V - 0.00048ED*RPM + 0.000027\ V*RPM \quad (4)$$

$$Colour_{AEC(mesh)} = 58.9 + 0.1863\ ET + 10.54\ ED + 0.601\ V + 0.00014\ RPM - 0.000002\ ET*ET - 1.01\ ED*ED - 0.00176\ Voltage*V + 0.000001\ RPM*RPM - 0.0656\ ET*ED - 0.00001\ ET*V - 0.000012\ ET*RPM - 0.113\ ED*V - 0.00002ED*RPM - 0.000052V*RPM \quad (5)$$

Under both EC and AEC circumstances, a color removal efficacy of 70% to 91% was attained for DSW utilizing Fe–Fe punched and mesh electrodes. The most important variables affecting color removal, according to the ANOVA findings, were Electrolysis Time (ET) and applied Voltage (V) ($p < 0.0001$). Figure 2's response surface plots show how applied voltage and ET work together to affect color removal effectiveness. Due to increased anodic dissolution of iron and the ensuing development of iron hydroxide flocs, which efficiently adsorb and destabilize colored compounds by sweep coagulation, an increase in both operating parameters improved color removal.

Similar trends have been reported by Chen (2004) and Shanmukha et al. (2020). Under EC conditions, the Fe–Fe punched electrode achieved colour removal efficiencies of approximately 78–88%, whereas the mesh electrode exhibited removals between 75–85% (Figure 2(a) and (b)).

The slightly better performance of the punched electrode can be attributed to improved local turbulence and enhanced mass transfer, which promoted efficient coagulant generation and pollutant destabilization. Comparable colour removal efficiencies (80–88%) using punched iron electrodes were also reported by Shanmukha et al. (2020). Aeration further improved the treatment performance, increasing the colour removal efficiency to 86–91% and 82–90% for the punched and mesh electrode configurations, respectively (Figure 2(c) and (d)). The faster oxidation of Fe^{2+} to Fe^{3+} is responsible for the improved performance, reduced electrode passivation, improved hydrodynamic mixing, and microbubble-assisted flotation, which facilitate the formation and separation of pollutant-laden flocs. The faster oxidation of Fe^{2+} to Fe^{3+} is responsible for the improved performance. Furthermore, the findings highlight that electrode geometry also influences treatment performance, with the Fe–Fe punched electrode exhibiting a marginal advantage under the investigated operating conditions.

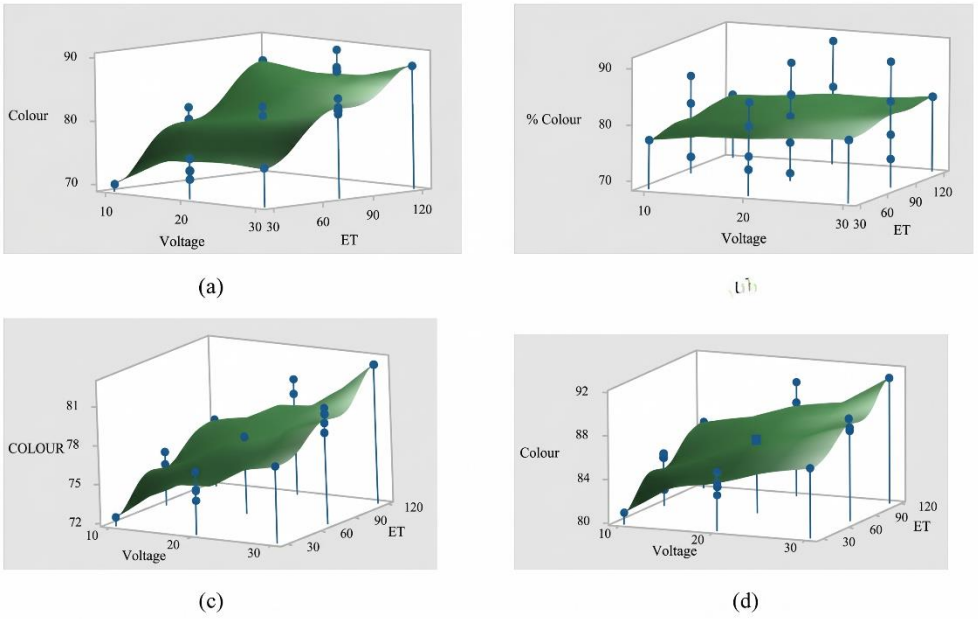


Fig. 2 Electrochemical treatment methods using Fe-Fe electrodes, (a) EC (punched), (b) EC (mesh), (c) AEC (punched), and (d) AEC (mesh) response surfaces and comparison graphs showing color removal effectiveness.

3.2. Optimization of COD Removal Efficiency

COD removal efficiencies ranging from 60 to 91% were obtained using Fe–Fe punched and mesh electrodes under EC and AEC conditions. Table 7 displays the experimental and anticipated COD removal efficiencies, and Appendix 1 (Tables 8 and 9) contains the related ANOVA findings. The ANOVA results confirmed that the developed models were statistically significant, with model F-values of 183.24 and 68.00 for the Fe–Fe punched electrode under EC and AEC, respectively, and 165.7 and 49.59 for the Fe–Fe mesh electrode. In all cases, the model p-values were < 0.0001, indicating the statistical significance of the developed models. Electrolysis Time (ET) and applied Voltage (V) were the most influential operating variables, with both showing highly significant effects ($p < 0.0001$). Inter-Electrode Distance (ED) also had a significant effect, whereas the influence of Agitation Speed (AS) was comparatively smaller and depended on the electrode configuration and treatment mode. Final regression equations for Fe-Fe (Punched-Plain and Mesh-Plain). For the EC and AEC processes using Fe–Fe punched, and mesh electrodes, the corresponding coded regression equations for COD removal are presented in Equations (6) to (9).

$$COD_{EC(punched)} = 62.57 + 0.1599\ ET - 1.92\ ED + 0.687\ V - 0.01287\ RPM - 0.000312\ ET*ET + 0.02\ ED*ED - 0.00140$$

V*V + 0.000008 RPM*RPM + 0.0093 ET*ED + 0.000111 ET*V + 0.000057 ET*RPM - 0.1000 ED*V + 0.00453ED*RPM-0.000380V*RPM (6)

$COD_{AEC(punched)}$= 59.78 + 0.1096 ET - 13.17 ED + 0.629 V+ 0.02088 RPM + 0.000104 ET*ET + 3.68 ED*ED + 0.00021V*V- 0.000011 RPM*RPM - 0.0077 ET*ED - 0.000200 ET*V- 0.000042 ET*RPM - 0.1040 ED*V-0.00150ED*RPM-0.000105V*RPM (7)

$COD_{EC(mesh)}$ = 99.57 + 0.0443 ET - 18.85 ED + 0.313 V + 0.00532 RPM + 0.000310 ET*ET + 3.01 ED*ED + 0.00227 V*V - 0.000005 RPM*RPM - 0.0398 ET*ED + 0.000078 ET*V + 0.000021 ET*RPM - 0.0900 ED*V-0.00277ED*RPM+0.000089V*RPM (8)

$COD_{AEC(mesh)}$ = 84.4 - 0.0425 ET - 0.02 ED + 0.011 V - 0.01311 RPM + 0.000132 ET*ET - 1.47 ED*ED + 0.00450 V*V + 0.000003 RPM*RPM + 0.0211 ET*ED + 0.00106 ET*V+ 0.000016 ET*RPM + 0.0210 ED*V+0.00583ED*RPM-0.000021V*RPM (9)

The response surface graphs in Figure 3 show how electrolysis time and voltage affect COD elimination. ET and voltage increased COD elimination overall. Increased anodic dissolution of iron and the production of iron hydroxide species enable adsorption, charge neutralization, and coagulation of dissolved and colloidal organic matter (Ponselvan et al. 2009; Chen, 2004; Kobya et al. 2003).

The close agreement between the experimental and predicted values presented in Table 7 further supports the adequacy of the developed response surface models.

Under the optimized condition of 120 min, 2 cm, 30 V and 600 rpm, the Fe–Fe mesh electrode achieved a maximum COD removal of 90.92% under AEC, with a predicted value of 89.71%.

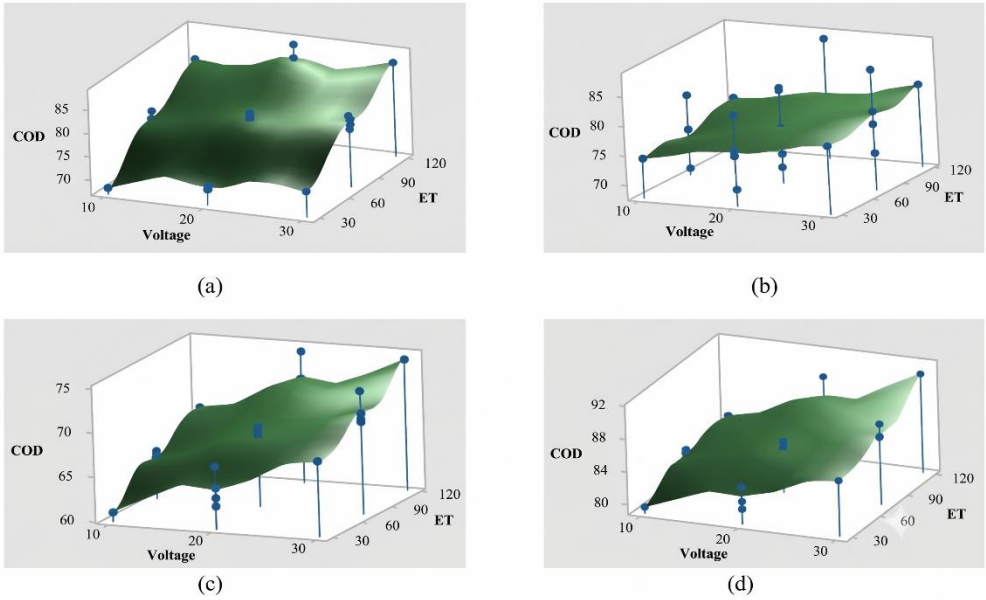


Fig. 3 Electrochemical treatment methods using Fe-Fe electrodes: (a) EC (punched), (b) EC (mesh), (c) AEC (punched), and (d) AEC (mesh) response surfaces and comparison graphs showing COD removal effectiveness.

Under EC conditions, the Fe–Fe punched electrode achieved COD removal efficiencies of approximately 60–80%, while the mesh electrode achieved 70–90%. The better performance of the mesh configuration indicates that electrode geometry influenced the treatment process. Its interconnected structure can promote electrolyte circulation and mass transfer near the electrode surface, facilitating contact between the generated iron species and organic pollutants. Thus, the observed improvement cannot be attributed to electrode surface area alone, but also to the geometry-dependent transport and electrochemical characteristics of the electrode. The introduction of aeration further enhanced COD removal, particularly for the Fe–Fe mesh configuration. The maximum removal of 90.92% obtained under AEC was comparable with the approximately 84% removal reported by Charles and Arunnellaiappan (2022) using twisted iron electrodes and the removals exceeding 90% reported by Nidheesh et al. (2020) under aerated EC conditions. Aeration can enhance the oxidation of Fe^{2+} to Fe^{3+}, improve mass transfer and mixing, and promote the flotation of pollutant-laden flocs through the formation of fine air bubbles (Mollah et al. 2001; Wang et al. 2021). The enhanced interaction between aeration and electrochemical reactions can therefore contribute to the improved COD removal observed under AEC conditions (Nidheesh and Omur, 2023). Overall, the RSM and ANOVA results presented in Appendix 1 (Tables 8 and 9) demonstrate

that electrolysis time and applied voltage were the dominant variables controlling COD removal, while electrode geometry and aeration also contributed to the treatment performance.

The Fe–Fe mesh electrode under AEC conditions provided the highest COD removal of 90.92%, demonstrating the effectiveness of combining the mesh electrode configuration with aeration for reducing the organic load of DSW.

3.3. Optimization of TDS Removal Efficiency

Various operating conditions influenced the removal of TDS from DSW. The observed and predicted TDS removal efficiencies obtained using Fe–Fe punched and mesh electrodes under EC and AEC conditions are presented in Table 10 (Appendix 1). Under the parameters under investigation, the TDS removal efficiency found in this research varied from around 50 to 89%. Equations (10)-(13) show the final coded regression equations that describe the link between the operational factors and TDS removal efficiency for the EC and AEC processes utilizing Fe–Fe punched and mesh electrodes.

- Final Regression equations for Fe-Fe (Punched-Plain and Mesh-Plain)

$TDS_{EC(punched)}$ = 85.58 + 0.1657 ET - 16.44 ED - 0.606 V - 0.01169 RPM + 0.000052 ET*ET+ 2.22 ED*ED + 0.00926 V*V + 0.000005 RPM*RPM - 0.0186 ET*ED - 0.000311 ET*V- 0.000016 ET*RPM + 0.2965 ED*V+ 0.00476ED*RPM-0.000208V*RPM (10)

$TDS_{AEC(punched)}$ = 59.59 + 0.1697 ET - 13.31 ED + 0.371 V - 0.00325 RPM + 0.000071 ET*ET + 1.817 ED*ED + 0.00539 V*V + 0.000000 RPM*RPM - 0.03256 ET*ED - 0.000011 ET*V - 0.000000 ET*RPM - 0.1695 ED*V+ 0.00263 ED*RPM + 0.000129 V*RPM (11)

$TDS_{EC(mesh)}$ =81.94 + 0.1159 ET - 21.03 ED + 0.490 Voltage 0.00451 RPM + 0.000053 ET*ET+ 3.27 ED*ED + 0.00277 Voltage*Voltage - 0.000002 RPM*RPM - 0.0322 ET*ED - 0.000411 ET*Voltage - 0.000019 ET*RPM - 0.2600 ED*Voltage - 0.00020 ED*RPM+ 0.000006 Voltage*RPM (12)

$TDS_{AEC(mesh)}$ = 57.09 + 0.0913 ET + 13.93 ED + 0.279 V + 0.00544 RPM - 0.000407 ET*ET - 3.56 ED*ED - 0.00425 V*V - 0.000004 RPM*RPM + 0.0072 ET*ED - 0.000600 ET*V + 0.000007 ET*RPM + 0.0825 ED*V + 0.00105ED*RPM+0.000014V*RPM (13)

Figure 4's response surface plots demonstrate how V and ET affect TDS elimination. Increasing ET and applied voltage generally improved TDS removal, which is explained by increased iron anodic dissolution and the consequent generation of $Fe(OH)_3$ coagulant species. These species facilitate the aggregation, adsorption, charge neutralization, sweep flocculation, and co-precipitation of dissolved and colloidal constituents, thereby improving TDS removal (Kobya et al. 2003; Chen, 2004). Under EC conditions, TDS removal efficiencies of approximately 65–80% and 60–75% were obtained for the punched and mesh electrodes, respectively, while under AEC conditions, the corresponding removal efficiencies increased to approximately 70–88% and 68–84%, respectively.

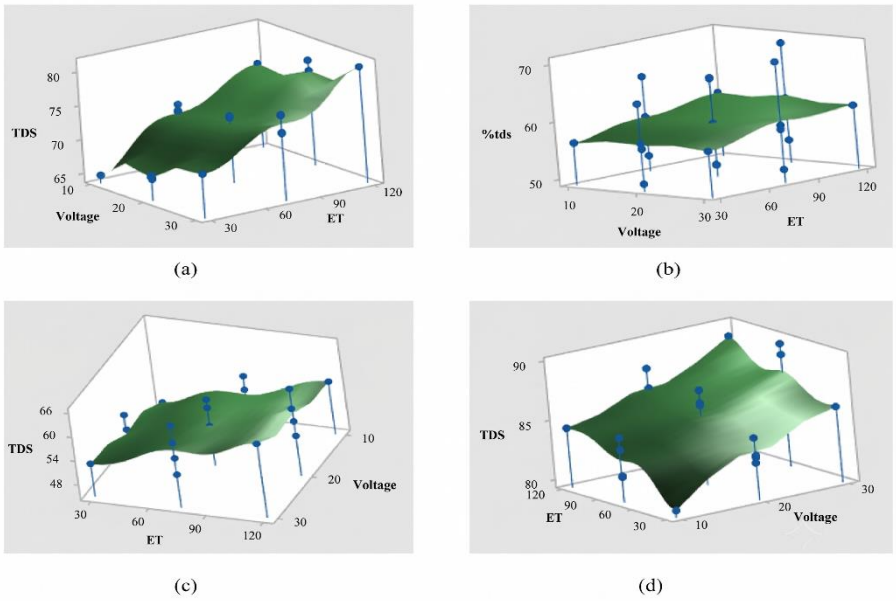


Fig. 4 Electrochemical treatment methods using Fe-Fe electrodes: (a) EC (punched), (b) EC (mesh), (c) AEC (punched), and (d) AEC (mesh) response surfaces and comparison graphs showing TDS removal effectiveness.

Compared with colour and COD removal, the response surfaces for TDS exhibited a relatively gradual variation with ET and applied voltage. This indicates that TDS removal is governed primarily by physicochemical processes such as adsorption, ionic entrapment, precipitation, and co-precipitation, rather than by direct degradation of dissolved organic compounds. The incorporation of dissolved constituents such as sulphates, chlorides, and other inorganic and organic salts into the iron hydroxide flocs may contribute to their subsequent separation from the treated wastewater. The introduction of aeration further improved TDS removal, with an improvement of approximately 5–10% compared with EC under the investigated conditions. This enhancement may be attributed to improved hydrodynamic mixing, accelerated oxidation of Fe^{2+} to Fe^{3+}, and microbubble-assisted flotation of the generated flocs. Aeration can therefore improve the contact between the wastewater constituents and the generated iron hydroxide species and facilitate their subsequent separation. Similar improvements associated with aerated electrochemical treatment have been reported in previous studies (Aatif et al. 2024; Wang et al. 2021; Emamjomeh and Sivakumar, 2009; Zongo et al. 2009). The ANOVA results presented in Tables 11 and 12 (Appendix 1) confirmed that the developed models were statistically significant ($p < 0.0001$) for both electrode configurations (Ramanathan et al., 2024). For the Fe–Fe punched electrode, the model F-values were 88.82 and 399.47 under EC and AEC, respectively, while the corresponding values for the Fe–Fe mesh electrode were 231.73 and 45.23.

Electrolysis time and applied voltage were significant factors under both EC and AEC conditions. The effects of electrode spacing and agitation speed varied depending on the electrode configuration and treatment condition. Overall, the results demonstrate that AEC provided improved TDS removal compared with conventional EC, particularly at higher electrolysis times and applied voltages. The findings also indicate that TDS removal depends on the combined effects of operating conditions, aeration, and electrode geometry. The observed performance demonstrates the potential of the Fe–Fe electrode-based EC/AEC process for reducing dissolved constituents in DSW

3.4. Scanning Electron Microscopy (SEM)

SEM was used to examine the surface morphology of the Fe–Fe electrodes before and after electrochemical treatment. The SEM images are presented in Figure 5. Before treatment, the electrode surface appeared relatively smooth and homogeneous, with minor machining marks and no noticeable deposits or corrosion products (Figure 5(a)).

After treatment, significant morphological changes were observed, with the electrode surface becoming rough and heterogeneous and exhibiting microcracks, irregular deposits, and flake-like structures (Figure 5(b)). Layered and fibrous aggregates were also observed at higher magnification, which have been associated with the formation of iron hydroxide and oxide complexes during anodic iron dissolution (Shaban et al. 2023).

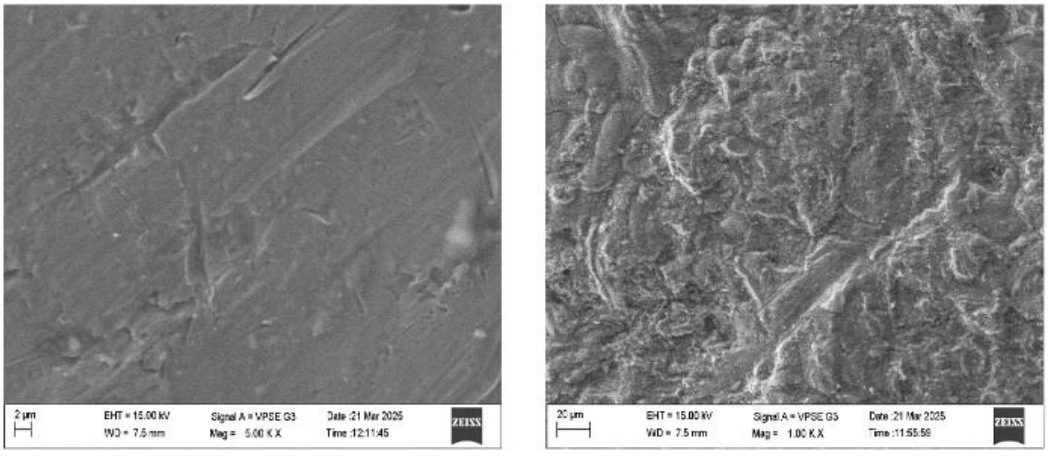


Fig. 5 SEM analysis of Iron electrode (a) SEM analysis of electrode before treatment, and (b) SEM analysis of Electrode after treatment.

The increased surface roughness and porous deposits indicate the occurrence of electrochemical reactions and localized corrosion during treatment. The accumulation of corrosion products and precipitated flocs on the electrode surface suggests the formation and deposition of iron-based coagulant species during the electrochemical process. These surface modifications can enhance the interaction between the generated coagulant species and wastewater constituents, thereby contributing to pollutant destabilization and removal. Similar morphological changes have been reported for iron-based EC systems, where the formation of iron hydroxide species is associated with electrode surface degradation and

contaminant removal (Muhammad et al., 2024). Overall, the SEM images provide morphological evidence of electrode dissolution, surface modification, corrosion, and deposition of reaction products during electrochemical treatment.

The observed transformation from a relatively smooth surface before treatment to a rough and deposit-covered surface after treatment supports the occurrence of iron-based electrochemical reactions and floc deposition. The corresponding changes in elemental composition were further investigated using EDX analysis, presented in Section 3.5.

3.5 Energy Dispersive X-ray Spectroscopy (EDX)

EDX was used to compare the elemental composition of the Fe–Fe electrode surface before and after electrochemical treatment (Figure 6). Before treatment, Iron (Fe) dominated the EDX spectra, with Oxygen (O), Carbon (C), Aluminum (Al), Silicon (Si), and Chlorine (Cl) intensities lower. The presence of minor elements may be associated with surface oxides, impurities, or traces originating from electrode preparation and storage. Electrochemical treatment increased oxygen and decreased Fe signals. This alteration suggests that electrochemical treatment increases oxygen-containing surface deposits and iron oxide/hydroxide-rich corrosion products on the electrode surface. Corrosion products and precipitated flocs partially cover the electrode surface, reducing the Fe signal (Million, 2021). The appearance or increased intensity of elements such as Cl and Zn after treatment may indicate the deposition or adsorption of constituents originating from the DSW on the electrode surface. The EDX results are consistent with the morphological changes observed by SEM in Figure 5, where the treated electrode exhibited increased surface roughness and deposited material. The combined SEM–EDX observations therefore provide evidence of electrode surface modification, iron dissolution, oxidation, and deposition of treatment-related species during EC/AEC treatment. Similar surface transformations associated with iron dissolution and oxide–hydroxide deposition have been reported for iron-based EC systems (Shaban et al. 2023). However, the specific chemical phases of the deposited iron species cannot be distinguished solely from EDX analysis and would require complementary techniques such as FTIR or XRD for definitive identification.

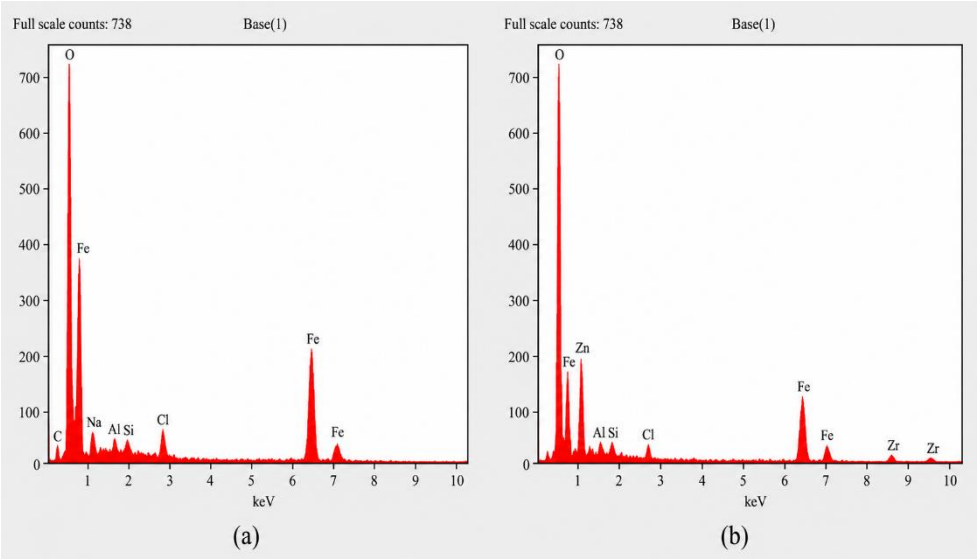


Fig. 6 EDX spectra of Iron electrode (a) Before treatment, and (b) After treatment.

3.6. Cost Analysis

EC is vital for DSW treatment without chemicals, and estimating the total operating cost is necessary (Kobya et al., 2020; Ebba, 2021; Nguyen, 2021). EC and AEC Operating Costs (OC) were estimated to assess cost-effectiveness. OC includes energy and electrode costs (Equation 14), Akter and Shahinoor (2022).

$$OC = a\ Cenergy + b\ Celectrod \quad (14)$$

In the equation, Cenergy represents energy consumption (kWh/m3), Celectrode represents electrode consumption (kg/m3), Cpump represents EC aeration (kWh/m3), and a and b represent energy and electrode material unit costs (₹/kWh and ₹/Kg); Energy unit cost (a) was set at 7₹/kWh, while iron material unit cost (b) at 70₹/Kg. Cenergy, Celectrode, and Cpump formulas are Equation (15)-(17) (Kobya et al., 2020; Martinez-Villafa et al., 2009).

$$C_{energy} = \frac{U \times i \times t}{1000} \quad (15)$$

$$C_{electrode} = \frac{i \times t \times M}{z \times F} \quad (16)$$

$$C_{pump} = \frac{9.81 \times h}{3600 \times \eta} \quad (17)$$

U is the applied Voltage (V), i is the applied Current (A), z is the number of electrons involved in the oxidation/reduction process (z=3), M is the Fe electrode's molecular weight (55.85 g/mol), t is the treatment duration (h), and F is Faraday's constant. Treatment methods are used based on efficacy and cost. This study calculated the OC under optimal operating circumstances (i=2A, t=2hr, U=20V). The highest electrode and power consumption for both electrode combinations throughout the testing run is 0.77 kg/m^3 and 0.08 kWh/m^3, respectively. The estimated Cpump for aeration is 0.0158 ₹/m^3. Based on energy and electrode usage, the OC of EC and AEC was determined to be 54.46 ₹/m3 and 54.48 ₹/m^3, respectively.

Limitations of the present study: Although SEM-EDS characterization was used to support the discussion of electrode surface changes and elemental composition, additional techniques such as FTIR and GC-MS were not performed to identify specific functional groups or degradation products. A formal Life-Cycle Assessment (LCA) and a comprehensive comparison of removal efficiency, energy efficiency, operating cost, and sludge characteristics with established electrodes, such as Al- and Ti-based electrodes, were also beyond the scope of this laboratory-scale study. Future studies should therefore include detailed molecular characterization, systematic comparison of different electrode materials, sludge characterization, and LCA to provide a more comprehensive assessment of treatment performance and environmental sustainability.

4. Conclusion

With significant decreases in color, COD, and TDS, the current research proved the efficacy of EC and AEC procedures using Fe–Fe punched and mesh electrodes for the treatment of DSW (DSW). Overall, colour and COD removal efficiencies ranged from 70–91% and 60–91%, respectively, while TDS removal varied between 50–89%, depending on the treatment process and electrode configuration. Among the electrode geometries investigated, the Fe-Fe mesh electrode consistently outperformed the punched electrode under all operating conditions, particularly during the AEC process. Despite having a comparatively lower nominal surface area, the mesh configuration exhibited superior pollutant removal due to improved availability of active sites, enhanced current distribution, and efficient generation of iron hydroxide flocs. The maximum removal efficiencies were achieved using the AEC process with Fe–Fe mesh electrodes, attaining 91.31% colour removal, 90.92% COD removal, and 89.70% TDS removal under the optimum operating conditions of 30 V applied voltage and 120 min electrolysis time. Optimization using RSM based on the BBD indicated that ET and applied voltage V were the most significant factors influencing treatment efficiency, whereas ED and AS showed relatively lower effects. The ANOVA results further confirmed the statistical significance of the developed models for colour, COD, and TDS removal, with p-values less than 0.001.

Following treatment, SEM and EDX analyzes showed significant surface change of the electrodes, including the deposition of pollutant-associated species and the creation of oxide–hydroxide layers. Active electrochemical reactions and efficient pollutant adsorption during the EC/AEC procedures were verified by the significant rise in oxygen content and the presence of elements like Cl and Zn.

These findings confirmed iron electrodes' critical function in coagulation and pollution removal processes. The economic viability of both systems was shown by the anticipated running costs of the EC and AEC processes, which were ₹54.46/m^3 and ₹54.48/m^3, respectively. Overall, the research shows that electrode shape and configuration have a major impact on process economics, operational efficiency, and treatment success; the Fe–Fe mesh electrode shows the most promising behavior. The results emphasize how crucial electrode adjustment is to improving the efficiency and long-term viability of electrochemical treatment systems for DSW remediation.

Conflicts of Interest

The authors declares that there is no conflict of interest regarding the publication of this paper.

Acknowledgments

Visvesvaraya Technological University, Belagavi in Karnataka, India, awarded the JanaYana Doctoral Fellowship, which helped fund the research.

References

[1] Aatif Ali Shah, Sunil Walia, and Hossein Kazemian, “Advancements in Combined Electrocoagulation Processes for Sustainable Wastewater Treatment: A Comprehensive Review of Mechanisms, Performance, and Emerging Applications,” *Water Research*, vol. 252, pp. 1-22, 2024. [CrossRef] [Google Scholar] [Publisher Link]

[2] Abhijeet Kumar, P.V. Nidheesh, and M. Suresh Kumar, “Composite Wastewater Treatment by Aerated Electrocoagulation and Modified Peroxi-Coagulation Processes,” *Chemosphere*, vol. 205, pp. 587-593. 2018. [CrossRef] [Google Scholar] [Publisher Link]

[3] Sonia Akter, and Md. Shahinoor Islam, “Effect of Additional Fe^{2+} Salt on Electrocoagulation Process for the Degradation of Methyl Orange Dye: An Optimization and Kinetic Study,” *Heliyon*, vol. 2, no. 8, pp. 1-15, 2022. [CrossRef] [Google Scholar] [Publisher Link]

[4] *Standard Methods for the Examination of Water and Wastewater*, American Public Health Association, American Water Works Association, Water Environment Federation, 2012. [Google Scholar] [Publisher Link]

[5] Terefe Tafese Bezuneh, "The Role of Microorganisms in Distillery Wastewater Treatment: A Review," *Journal of Bioremediation & Biodegradation*. vol. 7, no. 6, pp. 1-7, 2016. [CrossRef] [Publisher Link]

[6] Chantaraporn Phalakornkule et al., "Electrocoagulation of Blue Reactive, Red Disperse and Mixed Dyes, and Application in Treating Textile Effluent," *Journal of Environmental Management*, vol. 91, no. 4, pp. 918-926, 2010. [CrossRef] [Google Scholar] [Publisher Link]

[7] Charles David, Karpagaraj A, and Arunnellaiappan Thangavelu, "Degradation of Distillery Effluent by Twisted-Type Iron Electrodes: Experimental with ANN Approach," *International Journal of Environmental Analytical Chemistry*, vol. 102, no. 18, pp. 6121-6133, 2022. [CrossRef] [Google Scholar] [Publisher Link]

[8] Guohua Chen, "Electrochemical Technologies in Wastewater Treatment," *Separation and Purification Technology*, vol. 38, no. 1, pp. 11-41, 2004. [CrossRef] [Google Scholar] [Publisher Link]

[9] Madhuri Damaraju et al., "Treatment of Distillery Wastewater in a Bipolar-Mode Electrocoagulation System: Performance Evaluation and Kinetic Analysis," *International Journal of Civil Engineering*, vol. 17, no. 11, pp. 1643-1652, 2019. [CrossRef] [Google Scholar] [Publisher Link]

[10] Charles David et al., "Strategy for Enhanced Treatment of Distillery Spent Wash Effluent with Aluminum Nanoparticle-Assisted Electrocoagulation," *Chemical Engineering Communications*, vol. 212, no. 11, pp. 1750-1764, 2025. [CrossRef] [Google Scholar] [Publisher Link]

[11] Million Ebba, Perumal Asaithambi, and Esayas Alemayehu, "Investigation on Operating Parameters and Cost Using an Electrocoagulation Process for Wastewater Treatment," *Applied Water Science*, vol. 11, pp. 1-9, 2021. [CrossRef] [Google Scholar] [Publisher Link]

[12] Mohammad. M. Emamjomeh, and Muttucumaru. Sivakumar, "Review of Pollutants Removed by Electrocoagulation and Electrocoagulation/Flotation Processes," *Journal of Environmental Management*, vol. 90, no. 5, pp. 1663-1679, 2009. [CrossRef] [Google Scholar] [Publisher Link]

[13] Gaogui Jing et al., "Electrocoagulation in a Packed Aluminium Scraps Anode Reactor for Mineral Processing Wastewater Treatment," *Mineral Engineering*, vol. 202, pp. 1-4, 2023. [CrossRef] [Google Scholar] [Publisher Link]

[14] Waheed Ali Khokhar, Muhammad Rizwan, and Naveed Ahmed Qambrani, "Treatment of Anaerobically Digested Distillery Spent Wash Using Electrocoagulation with Al-SS-Al Electrode Configuration," *Water, Air, & Soil Pollution*, vol. 234, pp. 1-12, 2023. [CrossRef] [Google Scholar] [Publisher Link]

[15] Mehmet Kobya, Orhan Taner Can, and Mahmut Bayramoglu, "Treatment of Textile Wastewater by Electrocoagulation Using Iron and Aluminum Electrodes," *Journal of Hazardous Materials*, vol. 100, no. 1-3, pp. 163-178. 2003. [CrossRef] [Google Scholar] [Publisher Link]

[16] Mehmet Kobya, Philip Isaac Omwene, and Zubeda Ukundimana, "Treatment and Operating Cost Analysis of Metalworking Wastewaters by a Continuous Electrocoagulation Reactor," *Journal of Environmental Chemical Engineering*, vol. 2, no. 2, pp. 1-8, 2020. [CrossRef] [Google Scholar] [Publisher Link]

[17] B.M. Krishna et al., "Electrochemical Pretreatment of Distillery Wastewater using Aluminum Electrode," *Journal of Applied Electrochemistry*, vol. 40, pp. 663-673, 2010. [CrossRef] [Google Scholar] [Publisher Link]

[18] Mayank Kumar et al., "Treatment of Biodigester Effluent by Electrocoagulation using Iron Electrodes," *Journal of Hazardous Materials*, vol. 165, no. 1-3, pp. 345-352, 2009. [CrossRef] [Google Scholar] [Publisher Link]

[19] J.F. Martínez-Villafañe, C. Montero-Ocampo, and A.M. García-Lara, "Energy and Electrode Consumption Analysis of Electrocoagulation for the Removal of Arsenic From Underground Water," *Journal of Hazardous Material*, vol. 172, no. 2-3, pp. 1617-1622, 2009. [CrossRef] [Google Scholar] [Publisher Link]

[20] B. Merzouk et al., "Removal of Turbidity and Separation of Heavy Metals using Electrocoagulation–Electroflotation Technique: A Case Study," *Journal of Hazardous Materials*, vol. 164, no. 1, pp. 215-222, 2009. [CrossRef] [Google Scholar] [Publisher Link]

[21] M.Yousuf A Mollah et al., "Electrocoagulation (EC) — Science and Applications," *Journals of Hazardous Materials*, vol. 84, no. 1, pp. 29-41, 2001. [CrossRef] [Google Scholar] [Publisher Link]

[22] Million Ebba Bote, "Studies on Electrode Combination for COD Removal From Domestic Wastewater Using Electrocoagulation," *Heliyon*, vol. 7, pp. 1-6, 2021. [CrossRef] [Google Scholar] [Publisher Link]

[23] Muhammad Ghozali Harahap et al., "Electrocoagulation for Nickel, Chromium, and Iron Removal from Mine Water using Aluminum Electrodes," *Heliyon*, vol. 10, no. 23, pp. 1-13, 2024. [CrossRef] [Google Scholar] [Publisher Link]

[24] Duc Dat Duc Nguyen et al., "The Treatment of Real Dyeing Wastewater by the Electro-Fenton Process using Drinking Water Treatment Sludge as a Catalyst," *RCS Advances*, vol. 11, no. 44, pp. 27443-27452, 2021. [CrossRef] [Google Scholar] [Publisher Link]

[25] P.V. Nidheesh, and Ömür Gökkuş, "Aerated Iron Electrocoagulation Process as an Emerging Treatment Method for Natural Water and Wastewater," *Separation Science and Technology*, vol. 58, no. 11, pp. 2041-2063, 2023. [CrossRef] [Google Scholar] [Publisher Link]

[26] P.V. Nidheesh et al., "Treatment of Mixed Industrial Wastewater by Electrocoagulation and Indirect Electrochemical Oxidation," *Chemosphere*, vol. 251, pp. 1-10, 2020. [CrossRef] [Google Scholar] [Publisher Link]

[27] F. Infant Anto Ponselvan et al., "Electrocoagulation Stuides on Treatment of Biodigester Effluent using Aluminum Electrode," *Water Air Soil Pollution*, vol. 199, pp. 371-379, 2009. [CrossRef] [Google Scholar] [Publisher Link]

[28] Jelena Radjenovic, and David L. Sedlak, "Challenges and Opportunities for Electrochemical Processes as Next-Generation Technologies for the Treatment of Contaminated Water," *Environmental Science & Technology*, vol. 49, no. 19, pp. 11292-11302, 2015. [CrossRef] [Google Scholar] [Publisher Link]

[29] Giriprasath Ramanathan, Masroora Hassan, and Yury Rochev, "Optimising the Viscoelastic Properties of Hyaluronic Acid Hydrogels through Colloidal Particle Interaction: A Response Surface Methodology Approach," *Collids and Surfaces A: Physicochemical and Engineering Aspects*, vol. 703, no. 2, pp. 1-10, 2024. [CrossRef] [Google Scholar] [Publisher Link]

[30] A. Shaban, M.E. Basiouny, and Osama A. AboSiada, "Evaluation of Using Sequential Electrocoagulation and Chemical Coagulation for Urea Removal from Synthetic and Domestic Wastewater," *Water, Air and Soil Pollution*, vol. 234, pp. 1-14, 2023. [CrossRef] [Google Scholar] [Publisher Link]

[31] K. Chayashree, B. Lokeshappa, and N.T. Shanmukha, "Study of Cod and Colour Removal from Distillery Spent Wash using AL-AL Electrode in Electrocoagulation Process," *International Research Journal of Engineering and Technology (IRJET)*, vol. 7, no. 7, pp. 2659-2662, 2020. [Publisher Link]

[32] Tanim Arpit Singh et al., "Bioremediation of Melanoidin Contamination in Distillery Effluent using Aspergillus Brasiliensis," *BioTechnologia*, vol. 101, no. 3, pp. 205- 213, 2020. [CrossRef] [Google Scholar] [Publisher Link]

[33] Chandrakant Thakur, Vimal Chandra Srivastava, and Indra Deo Mall, "Electrochemical Treatment of a Distillery Wastewater: Parametric and Residue Disposal Study," *Chemical Engineering Journal*, vol. 148, no. 2-3, pp. 496-505, 2009. [CrossRef] [Google Scholar] [Publisher Link]

[34] Umran Tezcan Un, A. Savas Koparal, and Ulker Bakir Ogutveren, "Electrocoagulation of Vegetable Oil Refinery Wastewater using Aluminium Electrodes," *Journal of Environmental Management*, vol. 90, no. 1, pp. 428-433, 2009. [CrossRef] [Google Scholar] [Publisher Link]

[35] V. Khandegar, and Anil. K. Saroha, "Electrochemical Treatment of Distillery Spent Wash Using Aluminum and Iron Electrodes," *Chinese Journal of Chemical Engineering*, vol. 20, no. 3, pp. 439-443, 2012. [CrossRef] [Google Scholar] [Publisher Link]

[36] Rahul Verma, Lal Mohan Kundu, and Lalit M. Pandey, *Decontamination of Distillery Spent Wash Through Advanced Oxidation Methods*, Advanced Oxidation Processes for Effluent Treatment Plants, pp. 103-117, 2021. [CrossRef] [Google Scholar] [Publisher Link]

[37] Yong Wang et al., "Interactions between Flocs and Bubbles in the Separation Zone of Dissolved Air Flotation System," *Science of the Total Environment*, vol. 761, 2021. [CrossRef] [Google Scholar] [Publisher Link]

[38] Inoussa Zongo et al., "Removal of Hexavalent Chromium from Industrial Wastewater by Electrocoagulation: A Mechanistic Study," *Separation and Purification Technology*, vol. 66, no. 1, pp. 159-166, 2009. [CrossRef] [Google Scholar] [Publisher Link]

Appendix 1

Table 4. Observed and predicted performance of EC and AEC for COD removal using Fe-Fe punched and mesh electrodes

Fe-Fe (Colour Removal)				Punched Electrode				Mesh Electrode			
ET	ED	V	AS	EC (%)		AEC (%)		EC (%)		AEC (%)	
				Observed Value	Predicted Value	Observed Value	Predicted Value	Observed Value	Predicted Value	Observed Value	Predicted Value
75	2	30	300	82.53	81.4	80.17	79.81	77.74	78.47	89.10	88.88
75	2.5	30	600	82.19	82.45	79.52	79.40	73.47	73.73	88.36	88.44
75	2	10	900	80.72	79.51	74.98	74.64	80.98	81.04	84.21	83.27
30	2	30	600	75.06	75.45	77.64	77.92	79.69	79.99	86.23	86.64
30	1.5	20	600	73.3	73.46	75.10	75.75	85.2	86.01	84.34	84.28
75	2.5	20	300	79.11	79.23	76.55	76.79	69.67	69.65	85.99	85.81
120	2	20	900	89.61	88.68	79.57	79.15	82.26	83.6	88.42	88.15
75	1.5	20	300	80.67	79.4	77.78	77.64	83.76	84.49	86.39	86.51
75	2	20	600	79.31	80.45	77.68	77.23	79.75	79.75	85.97	86.08
30	2	20	300	72.11	72.23	74.40	75.31	75.47	75.91	83.15	84.01
75	2	10	300	78.97	77.23	75.90	74.62	75.48	75.67	84.65	83.44
75	2.5	20	900	82.26	81.51	76.77	76.82	75.07	75.02	85.84	85.64
120	2	30	600	88.49	89.62	81.46	81.73	81.78	82.31	91.31	90.95
120	2	10	600	86.67	85.45	76.85	76.53	79.56	79.52	85.93	85.51
30	2.5	20	600	73.51	73.28	76.66	74.90	73.16	71.17	85.31	83.57
75	2	20	600	79.31	80.45	77.68	77.23	79.75	79.75	85.97	86.08
75	2.5	10	600	77.07	78.28	74.19	74.21	71.29	70.94	82.71	83.00
75	1.5	10	600	77.66	78.45	73.66	75.05	85.76	85.78	81.31	83.71
30	2	10	600	70.16	71.29	72.37	72.73	77.17	77.2	80.84	81.20
120	1.5	20	600	86.68	87.62	80.65	79.55	90.41	88.34	90.25	88.58
75	2	30	900	84.78	83.68	78.71	79.84	83.56	83.84	88.04	88.71
75	1.5	30	600	83.22	82.62	80.63	80.25	90.77	88.57	89.23	89.15
120	2.5	20	600	86.88	87.45	76.75	78.71	73.65	73.5	85.32	87.88
75	1.5	20	900	80.55	81.68	77.66	77.66	89.45	89.86	86.25	86.35
75	2	20	600	79.97	80.45	77.68	77.23	79.75	79.75	86.71	86.08
30	2	20	900	75.24	74.51	75.20	75.34	80.91	81.28	83.86	83.84
120	2	20	300	86.1	86.4	77.92	79.12	77.87	78.23	88.34	88.31

Table 5. ANOVA - based evaluation of colour removal efficiency (Fe-Fe punched)

Source	DF		Adj SS		F-Value		P-Value	
	EC	AEC	EC	AEC	EC	AEC	EC	AEC
Model	4	4	669.93	126.54	161.38	39.17	<0.0001	<0.0001
Linear	4	4	669.93	126.54	161.38	39.17	<0.0001	<0.0001
ET	1	1	602.09	2.12	112.2	10.63	<0.0001	0.0119
ED	1	1	0.088	43.45	20.33	53.81	0.0774	<0.0001
V	1	1	52.15	80.96	80.45	100.24	<0.0001	<0.0001
AS	1	1	15.59	1.02	6.44	2.0	0.0010	0.0956
Error	22	22	22.83	17.76				
Lack-of-fit	20	20	22.54	17.76				
Total	26	26	804.84	168.88				

Table 6. ANOVA - based evaluation of colour removal efficiency (Fe-Fe mesh)

Source	DF		Adj SS		F-Value		P-Value	
	EC	AEC	EC	AEC	EC	AEC	EC	AEC
Model	4	4	786.90	145.89	241.23	134.9	<0.0001	<0.0001
Linear	4	4	786.90	145.89	241.23	134.9	<0.0001	<0.0001
ET	1	1	660.67	1.49	112.43	53.25	<0.0001	<0.0001
ED	1	1	16.17	55.64	19.83	10.45	0.0005	0.0012

V	1	1	23.43	88.67	70.21	84.86	<0.0001	<0.0001
AS	1	1	86.61	0.08	5.44	3.67	0.0523	0.7800
Error	22	22	17.94	22.98				
Lack-of-fit	20	20	17.94	22.62				
Total	26	26	804.84	168.88				

Table 7. Observed and predicted performance of EC and AEC for COD removal using Fe-Fe punched and mesh electrodes

Fe-Fe (COD Removal)				Punched Electrode				Mesh Electrode			
				EC (%)		AEC (%)		EC (%)		AEC (%)	
ET	ED	V	AS	Observed Value	Predicted Value	Observed Value	Predicted Value	Observed Value	Predicted Value	Observed Value	Predicted Value
75	2	30	300	79.23	79.75	70.05	71.39	80.87	80.98	86.89	86.73
75	2.5	30	600	79.13	80.22	71.11	70.33	73.78	73.61	87.10	87.25
75	2	10	900	78.02	76.88	65.09	64.28	71.89	73.84	82.66	82.17
30	2	30	600	72.23	72.86	68.29	67.71	78.98	79.11	85.59	85.18
30	1.5	20	600	70.31	70.95	66.76	65.21	79.12	80.9	83.21	82.38
75	2.5	20	300	77.35	77.43	67.30	66.87	72.3	71.53	83.21	83.54
120	2	20	900	80.42	80.12	69.96	71.42	77.8	77.79	89.01	87.43
75	1.5	20	300	79.09	77.84	68.69	68.88	83.56	84.77	84.35	83.93
75	2	20	600	78.34	78.31	67.78	67.83	76.88	77.41	85.00	84.45
30	2	20	300	70.18	70.07	62.35	64.25	76.87	77.02	81.53	81.47
75	2	10	300	75.43	75.53	63.55	64.36	75.16	75.32	80.72	80.74
75	2.5	20	900	80.22	78.78	65.94	66.78	70.18	70.04	85.10	84.97
120	2	30	600	80.51	81.92	74.56	74.97	81.34	81.36	90.92	89.71
120	2	10	600	81.10	83.77	67.51	67.95	76.56	75.71	82.87	83.72
30	2.5	20	600	70.35	70.54	64.43	63.20	70.34	69.66	80.60	81.99
75	2	20	600	78.34	78.31	67.78	67.83	76.88	77.41	83.79	84.45
75	2.5	10	600	76.11	76	64.19	63.31	68.67	67.96	82.07	81.26
75	1.5	10	600	76.42	76.41	64.67	65.33	80.98	81.2	82.39	81.65
30	2	10	600	68.05	68.64	60.88	60.69	74.34	73.45	79.44	79.19
120	1.5	20	600	81.92	82.10	74.56	72.47	84.89	84.1	86.32	86.91
75	2	30	900	80.11	81.1	70.33	71.30	78.67	79.49	88.58	88.16
75	1.5	30	600	81.44	80.63	73.67	72.35	82.89	83.86	87.00	87.64
120	2.5	20	600	80.12	79.76	71.54	70.45	71.67	71.91	85.61	86.52
75	1.5	20	900	79.24	79.19	68.23	68.80	83.1	83.29	82.74	85.36
75	2	20	600	78.34	78.31	67.68	67.83	76.88	77.41	83.79	84.45
30	2	20	900	70.88	71.42	63.22	64.16	75.89	75.54	83.44	82.90
120	2	20	300	81.59	80.79	71.36	71.50	77.67	79.28	86.23	86.00

Table 8. ANOVA - based evaluation of COD removal efficiency (Fe-Fe punched)

Source	DF		Adj SS		F-Value		P-Value	
	EC	AEC	EC	AEC	EC	AEC	EC	AEC
Model	4	4	746.44	318.10	183.24	68	<0.0001	<0.0001
Linear	4	4	746.44	318.10	183.24	68	<0.0001	<0.0001
ET	1	1	0.50	158.05	674.52	135.15	<0.0001	<0.0001
ED	1	1	686.94	12.16	8.43	10.41	0.0010	0.0040
V	1	1	53.51	147.86	52.54	126.43	<0.0001	<0.0001
AS	1	1	5.48	0.023	5.39	0.02	0.0300	0.8900
Error	22	22	22.40	25.72				
Lack-of-fit	20	20	22.40	25.72				
Total	26	26	692.76	144.31				

Table 9. ANOVA - based evaluation of COD removal efficiency (Fe-Fe mesh)

Source	DF		Adj SS		F-Value		P-Value	
	EC	AEC	EC	AEC	EC	AEC	EC	AEC
Model	4	4	643.95	175.61	165.7	49.59	<0.0001	<0.0001
Linear	4	4	643.95	175.61	165.7	49.59	<0.0001	<0.0001
ET	1	1	526.15	0.44	541.56	69.38	<0.0001	<0.0001
ED	1	1	15.25	61.42	15.7	9.38	0.0010	0.0042
V	1	1	95.93	107.58	98.75	121.51	<0.0001	<0.0001
AS	1	1	6.60	6.163	6.79	6.96	0.0160	0.0150
Error	22	22	21.37	19.47				
Lack-of-fit	20	20	21.37	18.50				
Total	26	26	804.84	168.88				

Table 10. Observed and predicted performance of EC and AEC for TDS removal using Fe-Fe punched and mesh electrodes

Fe-Fe (TDS Removal)				Punched Electrode				Mesh Electrode			
				EC (%)		AEC (%)		EC (%)		AEC (%)	
ET	ED	V	AS	Observed Value	Predicted Value	Observed Value	Predicted Value	Observed Value	Predicted Value	Observed Value	Predicted Value
75	2	30	300	76.20	75.22	56.50	56.40	58.21	58.86	86.34	86.39
75	2.5	30	600	76.39	74.72	52.31	52.79	51.12	51.26	87.55	88.65
75	2	10	900	71.70	70.22	52.58	52.99	58.28	58.28	83.73	83.66
30	2	30	600	70.15	69.38	52.40	52.76	56.87	57.32	85.70	85.75
30	1.5	20	600	67.33	67.38	54.28	54.67	64.11	64.62	82.45	82.12
75	2.5	20	300	73.29	73.04	47.83	48.01	50.8	50.49	84.86	85.25
120	2	20	900	76.98	77.74	61.06	61.40	59.99	60.59	87.80	87.70
75	1.5	20	300	73.66	73.22	58.52	58.31	65.89	66.17	82.48	82.76
75	2	20	600	71.80	72.72	54.17	54.69	58.1	58.57	86.00	85.02
30	2	20	300	66.84	67.70	47.33	47.99	56.12	56.54	83.09	82.35
75	2	10	300	71.61	71.04	50.28	49.92	57.67	57.8	81.48	81.63
75	2.5	20	900	73.68	72.22	51.55	51.08	51.01	50.97	87.31	87.29
120	2	30	600	81.02	80.24	62.73	63.11	59.87	60.89	86.70	85.15
120	2	10	600	76.07	76.06	57.27	56.63	59.89	59.82	84.34	84.30
30	2.5	20	600	66.80	67.20	45.45	44.37	50.01	48.95	82.89	84.62
75	2	20	600	71.87	72.72	54.17	54.69	58.1	58.57	86.21	85.02
75	2.5	10	600	69.45	70.54	47.02	46.31	51.45	50.2	84.78	83.89
75	1.5	10	600	72.65	70.72	56.01	56.60	65.18	65.87	81.59	81.40
30	2	10	600	64.64	65.20	46.92	46.28	56.15	56.25	79.93	80.99
120	1.5	20	600	79.23	78.24	65.91	65.02	69.56	68.19	88.76	88.42
75	2	30	900	73.78	74.40	60.35	59.47	58.89	59.34	85.54	85.10
75	1.5	30	600	73.66	74.90	64.69	63.08	70.05	66.94	84.86	86.16
120	2.5	20	600	77.02	78.06	54.15	54.72	52.56	52.52	86.19	87.92
75	1.5	20	900	71.20	72.40	60.66	61.37	66.22	66.65	84.30	84.80
75	2	20	600	71.76	72.72	54.17	54.69	58.1	58.57	86.21	85.02
30	2	20	900	67.01	66.88	50.53	51.05	57.17	57.02	84.54	84.39
120	2	20	300	77.65	78.56	57.87	58.33	59.98	60.11	85.99	85.66

Table 11. ANOVA-based evaluation of TDS removal efficiency (Fe-Fe punched)

Source	DF		Adj SS		F-Value		P-Value	
	EC	AEC	EC	AEC	EC	AEC	EC	AEC
Model	4	4	408.57	793.57	88.82	399.47	<0.0001	<0.0001
Linear	4	4	408.57	793.57	88.82	399.47	<0.0001	<0.0001
ET	1	1	354.01	321.32	100.5	215.44	<0.0001	<0.0001
ED	1	1	10.34	317.96	10.34	50.54	0.7710	0.0050
V	1	1	52.46	126.05	45.62	253.81	<0.0001	<0.0001

AS	1	1	1.99	28.22	1.73	5.68	0.2020	0.0500
Error	22	22	25.30	10.92				
Lack-of-fit	20	20	25.29	10.92				
Total	26	26	433.87	804.50				

Table 12. ANOVA-based evaluation of TDS removal efficiency (Fe-Fe mesh)

Source	DF		Adj SS		F-Value		P-Value	
	EC	AEC	EC	AEC	EC	AEC	EC	AEC
Model	4	4	779.60	131.74	231.73	45.23	<0.0001	<0.0001
Linear	4	4	779.60	131.74	231.73	45.23	<0.0001	<0.0001
ET	1	1	737.27	18.62	276.56	45.09	<0.0001	<0.0001
ED	1	1	38.23	32.83	45.46	25.58	0.0050	0.0010
V	1	1	3.40	67.87	115.55	93.21	<0.0001	<0.0001
AS	1	1	0.69	12.40	2.34	17.03	0.3730	0.0035
Error	22	22	18.50	16.02				
Lack-of-fit	20	20	18.50	15.99				
Total	26	26	798.11	147.76				